General Disclaimer

One or more of the Following Statements may affect this Document

- This document has been reproduced from the best copy furnished by the organizational source. It is being released in the interest of making available as much information as possible.

- This document may contain data, which exceeds the sheet parameters. It was furnished in this condition by the organizational source and is the best copy available.

- This document may contain tone-on-tone or color graphs, charts and/or pictures, which have been reproduced in black and white.

- This document is paginated as submitted by the original source.

- Portions of this document are not fully legible due to the historical nature of some of the material. However, it is the best reproduction available from the original submission.

NASA
Technical
Memorandum

NASA TM-82536

INSTRUMENTAL EFFECTS ON THE TEMPERATURE AND DENSITY DERIVED FROM THE LIGHT ION MASS SPECTROMETER

By Paul D. Craven and David L. Reasoner
Space Science Laboratory

June 1983

National Aeronautics and
Space Administration
George C. Marshall Space Flight Center

TECHNICAL REPORT STANDARD TITLE PAGE

1. REPORT NO.	2. GOVERNMENT ACCESSION NO.	3. RECIPIENT'S CATALOG NO.
NASA TM-82535		

4. TITLE AND SUBTITLE

Instrumental Effects on the Temperature and Density Derived from the Light Ion Mass Spectrometer

5. REPORT DATE June 1983

6. PERFORMING ORGANIZATION CODE

7. AUTHOR(S)

Paul D. Craven and David L. Reasoner

8. PERFORMING ORGANIZATION REPORT #

9. PERFORMING ORGANIZATION NAME AND ADDRESS

George C. Marshall Space Flight Center
Marshall Space Flight Center, Alabama 35812

10. WORK UNIT NO.

11. CONTRACT OR GRANT NO.

12. SPONSORING AGENCY NAME AND ADDRESS

National Aeronautics and Space Administration
Washington, D.C. 20546

13. TYPE OF REPORT & PERIOD COVERED

Technical Memorandum

14. SPONSORING AGENCY CODE

15. SUPPLEMENTARY NOTES

Prepared by Space Science Laboratory, Science and Engineering

16. ABSTRACT

An expression for the flux into an RPA is derived which takes into account the instrumental effect of a dependence on energy of the solid angle of the acceptance cone. A second instrumental effect of a limited bandpass is briefly discussed. Using the characteristics of the LIMS instrument on SCATHA, it is shown that temperatures and densities derived without considering the effect of the solid angle dependence on energy will be too low, dramatically so for $E_t > E_1$, where E_1 is the e folding distance of the solid angle dependence and E_t is the thermal energy of the plasma. For $E_t << E_1$, there is effectively no impact on the derived temperatures and densities if the solid angle effect is ignored.

17. KEY WORDS

Retarding Potential Analyzer
Mass Spectrograms
LIMS, SCATHA, Instrumental Effects

18. DISTRIBUTION STATEMENT

Paul D. Craven

Unclassified – Unlimited

19. SECURITY CLASSIF. (of this report)	20. SECURITY CLASSIF. (of this page)	21. NO. OF PAGES	22. PRICE
Unclassified	Unclassified	27	NTIS

TABLE OF CONTENTS

LIST OF ILLUSTRATIONS

LIST OF ILLUSTRATIONS (Concluded)

TECHNICAL MEMORANDUM

INSTRUMENTAL EFFECTS ON THE TEMPERATURE AND DENSITY DERIVED FROM THE LIGHT ION MASS SPECTROMETER

INTRODUCTION

In a recent article, Reasoner et al. [1] described the Light Ion Mass Spectrometer (LIMS) that was flown on the SCATHA satellite. This second-generation instrument was designed to measure the density, temperature, and flow velocity of low-energy ions ($E < 100$ eV). The instrument combined a retarding potential analyzer (RPA) with a magnetic mass spectrometer. Instrumental effects which are inherent in the design of the instrument are that the acceptance cone solid angle varies with mass and energy (Instrumental Effect A) and that the energy bandpass varies inversely as the mass (Instrumental Effect B). This report looks at how these effects influence flux measurements and derived temperatures and densities of the plasmas. A non-ramming, thermal plasma with a Maxwellian distribution is assumed in all the analysis. For the effects on the measured temperature and density, comparisons are made with the temperature and densities found using an instrument with a limited aperture ($\Omega < 2\pi$ steradian) but no acceptance cone energy dependence.

The acceptance cone angle of the LIMS instrument decreases with increasing ion energy and mass. The effect is such that, generally, the density and temperature of the plasma are underestimated if a constant solid angle is assumed in the analysis. However, there is a small range near zero temperature in which neither the temperature nor density is affected.

The effect of the mass-dependent energy bandpass is to reduce the flux for the higher mass ions when their energies are close to the limit of the bandpass.

PROBLEM DESCRIPTION AND SOLUTION

The instrument is described in the article by Reasoner et al. [1]. The detailed description will not be repeated here, but it is noted that the LIMS is a planar-type, retarding potential analyzer (RPA) followed by a magnetic mass spectrometer. The field-of-view of the instrument is cone shaped with geometrically-set limits such that the half angle of the cone is a maximum of 60 deg.

The energy passband of the instrument is determined by the fact that the mass resolution is given by:

$$\Delta M/M = 0.1 = C \quad . \tag{1}$$

However, since $E = kq/M$, it follows that:

$$\Delta M/M = -\Delta E/E = C \quad , \tag{2}$$

and therefore

$$\Delta E = -CE = -CKq/M = C'/M \quad . \qquad (3)$$

Thus, as the mass gets larger ΔE decreases. If the bandpass is rectangular from 0 to the upper energy limit, E_u, then for plasmas containing significant components with energy greater than E_u, only part of the plasma will be detected by the instrument. If, in addition, there is a lower energy limit, E_L, to detection se. by a retarding potential, as with an RPA device, then only that part of the plasma with energies between E_L and E_u will be detected. This is shown schematically in Figure 1 in which the bandpass transmission, T(E), is drawn on a plot of the distribution function versus energy. The flux with energies between E_L and E_u measured by the instrument can be expressed as:

$$F(E_L, E_u) = F(E_L, \infty) - F(E_u, \infty) \quad ,$$

where the first argument of F, E_L, is the lower energy limit and the second argument, E_u, is the upper energy limit of the flux integral, which will be discussed later. The fraction of the flux that is detected at an RPA equivalent to E_L is therefore:

$$R = F(E_L, E_u)/F(E_L, \infty) = 1 - F(E_u, \infty)/F(E_L, \infty) \quad . \qquad (4)$$

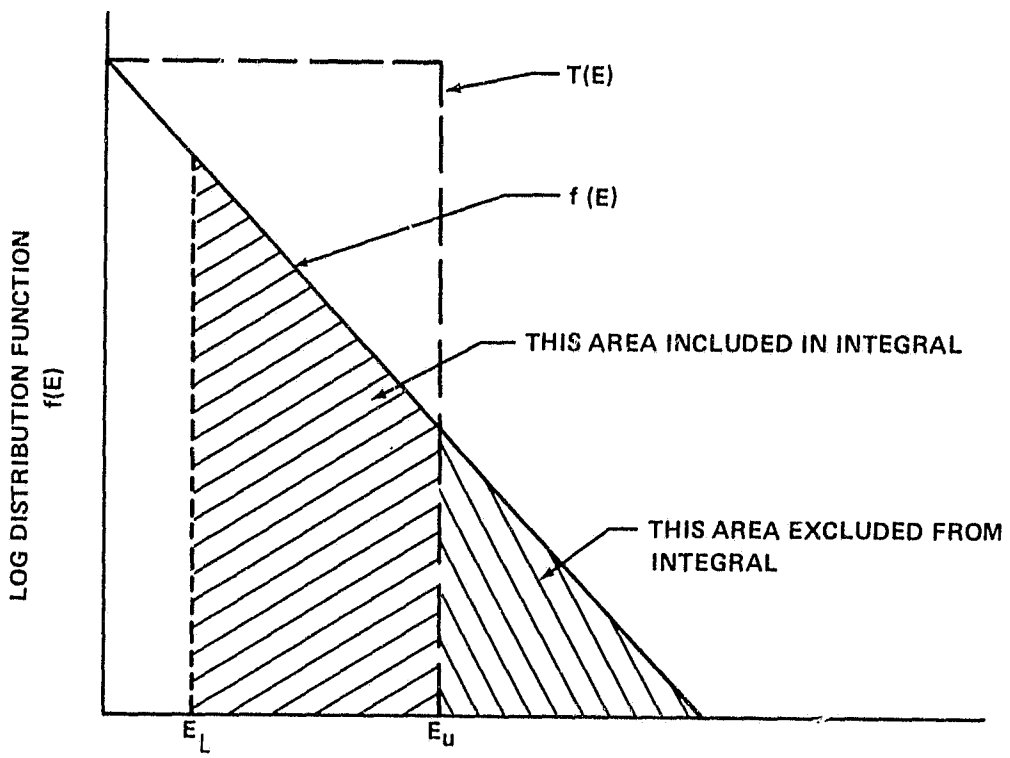

Figure 1. Schematic illustration of Instrumental Effect B on the flux integral.

Equation (4) expresses the fraction of the flux that is measured in terms of an RPA expression for the flux into the instrument; i.e., $F(E_u, \infty)$. Note that equation (4) is not the fraction of the total possible flux but the fraction of the flux into the instrument. If there are no instrumental effects, these two should be equal. The results of the bandpass will be seen in a plot of flux versus RPA potential energy as a falloff in flux even when the plasma energy is less than the bandpass cutoff and the flux will approach 0 as E_L approaches E_u. The effects of equation (4) on the RPA curves and therefore derived temperatures and densities will be discussed later.

The behavior of the solid angle acceptance of the LIMS/SCATHA instrument is shown in Figure 2 from Reasoner et al. [1] (their Figure 7). From this graph, it can be seen that a reasonable approximation to the behavior of the solid angle with respect to plasma energy, expressed in terms of velocity, is an exponential of the form:

$$\Omega = \Omega_o \exp\ (-V^2/V_1^2) \quad , \tag{5}$$

where

Ω = solid angle of the acceptance cone for plasma energy E,

Ω_o = the solid angle determined by the geometrical limits of the instrument,

V_1 = the characteristic velocity of the solid angle; i.e., the velocity at which the solid angle has decreased by a factor of e.

V_1 varies with the mass as mentioned earlier.

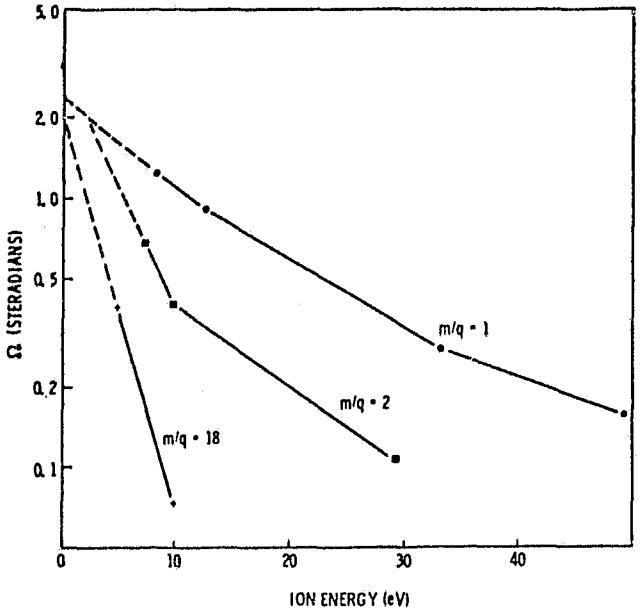

Figure 2. Computed values of the solid angle response Ω in steradians as a function of ion energy and mass.

Assuming a non-drifting Maxwellian distribution, the flux into a planar-type RPA instrument is given in spherical coordinates by:

$$\text{Flux} = (2nV_t/\sqrt{\pi}) \int_0^{\theta(V)} \int_{V=V_o/\cos\theta}^{\infty} \exp(-V^2/V_t^2)(V^3/V_t^3) \cos\theta \sin\theta d\theta \, d(V/V_t) \quad , \tag{6}$$

where

n = the density of the plasma,

V_t = the thermal velocity equivalent of the thermal energy of the plasma,

V_o = the velocity required to overcome the retarding potential,

θ = the angle between the normal to the instrument surface and the incoming velocity vector,

$\theta(V)$ = the maximum acceptance half angle for a given velocity,

V = the velocity of an ion.

The integration over the azimuth angle ϕ has been carried out in equation (6) assuming azimuthal symmetry.

A careful examination of the θ-V domain of the integral shows that there are regions of this space which are not accessible in the integral. Figure 3 shows these regions. Regions for which $\theta > \theta_{max}$ are not included in the integral due either to a limit imposed by the retarding potential or by the instrumental effect seen in the solid angle dependence on energy and expressed as $\theta_{max} = G(V)$. Notice there is a transition velocity, V', at which the limit on θ_{max} changes from that due to the retarding potential acting on the component of velocity parallel to the instrument normal to that due to the energy dependence of the solid angle. Reversing the order of integration, using the limits set as shown earlier and separating the integral over V into two parts, the flux integral becomes:

$$\text{Flux} = (2nV_t/\sqrt{\pi}) \int_{V=V_o}^{V'} \int_{\theta=o}^{\theta_{max}=\cos^{-1}(V_o/V)} [\quad] \, d(V/V_t) \, d\theta$$

$$+ \int_{V=V'}^{\infty} \int_{\theta=o}^{\theta_{max}=G(V)} [\quad] \, d(V/V_t) \, d\theta \quad , \tag{7}$$

where the integrand represented by the brackets remains the same as that in equation (6).

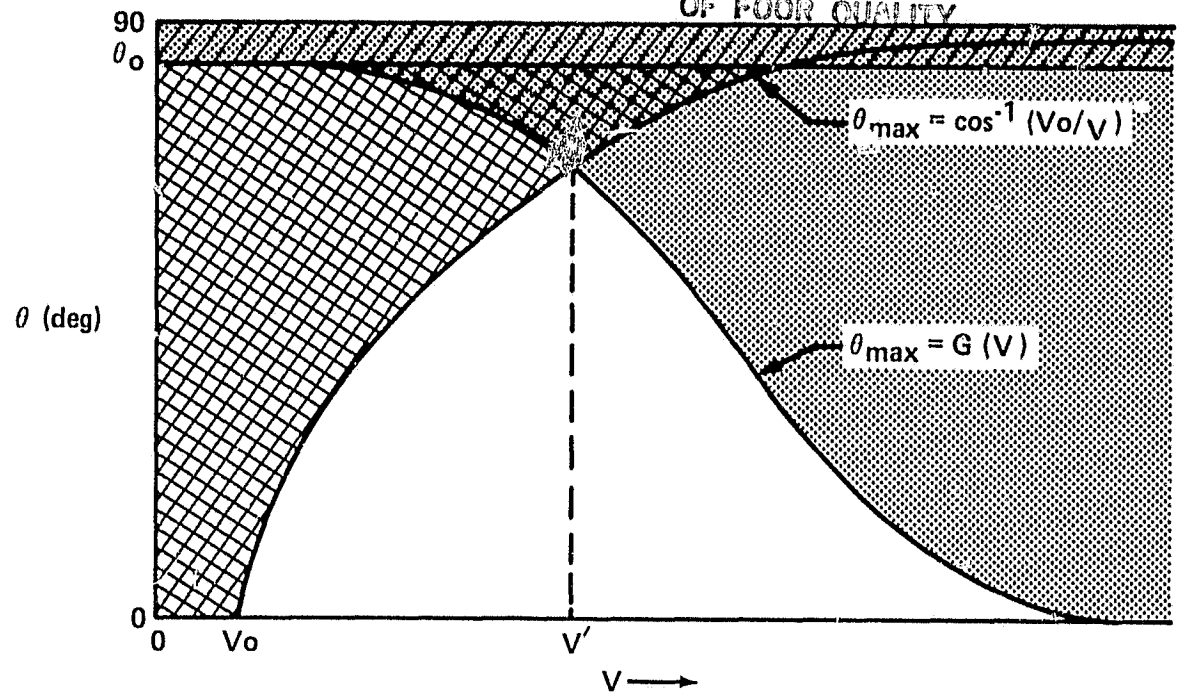

Figure 3. The different regions of θ - V space. Particles that have velocities with magnitudes and directions in the clear area contribute to the flux integral. Those that have velocities with magnitudes and direction in the stripped or stipled area do not. V' is the velocity magnitude at which the limits of integration change from being related to the RPA potential to being related to G(V).

Using the fact that

$$\Omega = 2\pi\,(1-\cos\theta) \text{ or } \cos\theta = 1 - \Omega/2\pi \quad ,$$

with the solid angle of the acceptance cone determined by the particle's velocity, the expression for G(V) can then be written:

$$G(V) = \theta_{max} = \cos^{-1}\,(1 - \Omega(V)/2\pi) \quad .$$

Using the variable change

$$\cos\theta \sin\theta\, d\theta = -\cos\theta\, d\,(\cos\theta) \quad ,$$

equation (7) can be written:

$$\text{Flux} = (2nV_t/\sqrt{\pi}) \int_{V_o}^{V'} \int_{\theta_{max}=\cos^{-1}(V_o/V)}^{1} \exp(-V^2/V_t^2)(V^3/V_t^3)\,d(V/V_t)\,\cos\theta\,d(\cos\theta)$$

$$+ (2nV_t/\sqrt{\pi}) \int_{V'}^{\infty} \int_{\theta_{max}=\cos^{-1}(1-\Omega(V)/2\pi)}^{1} \exp(-V^2/V_t^2)(V^3/V_t^3)\,d(V/V_t)\,\cos\theta d(\cos\theta)\ . \tag{8}$$

Integrating over $\cos\theta$ gives:

$$\text{Flux} = (nV_t/\sqrt{\pi}) \int_{V_o}^{V'} \exp(-V^2/V_t^2)(V^3/V_t^3)(1-V_o^2/V^2)\,d(V/V_t)$$

$$+ (nV_t/\sqrt{\pi}) \int_{V_o}^{V'} \exp(-V^2/V_t^2)(V^3/V_t^3)(1-(1-\Omega(V)/2\pi)^2)\,d(V/V_t)\ . \tag{9}$$

Whether the second part of this expression is analytically integrable or not depends on the form of $\Omega(V)$. For the form chosen here [equation (5)], equation (9) is analytically integrable.

Another change of variable is advantageous at this point. Let

$$Z = V^2/V_t^2 = E/E_t$$

$$Z_o = V_o^2/V_t^2 = E_o/E_t$$

$$Z' = (V'/V_t)^2 = E'/E_t$$

$$K = nV_t/\sqrt{\pi}\ ,\ = n\sqrt{2E_t/M\pi}\ ,$$

then equation (9) can be written:

$$\text{Flux} = \frac{K}{2}\int_{Z_o}^{Z'} \exp(-Z)Z\,dZ + \frac{KZ_o}{2}\int_{Z_o}^{Z'} \exp(-Z)\,dZ + \frac{K}{2}\int_{Z'}^{\infty} \exp(-Z)Z\,dZ + \frac{K}{2}\int_{Z'}^{\infty} \exp(-Z)\ Z(1-\Omega(Z)/2\pi)^2\,dZ\ . \tag{10}$$

The transformation of $\Omega(V)$ to $\Omega(Z)$ is as follows:

$$1 - \Omega(V)/2\pi = 1 - (\Omega_o/2\pi) \exp(-V^2/V_1^2) = 1 - (\Omega_o/2\pi) \exp(-ZV_t^2/V_1^2) \quad .$$

Let $(V_1/V_t)^2 = Z_1 = E_1/E_t$, then:

$$1 - \Omega(V)/2\pi = 1 - (\Omega_o/2\pi) \exp(-Z/Z_1) = 1 - \Omega(Z)/2\pi \quad . \tag{11}$$

Using equation (11), expanding $(1 - \Omega(Z)/2\pi)^2$, and integrating all terms, equation (10) reduces to:

$$\text{Flux} = \frac{K}{2}\left[(Z_o+1)\, e^{-Z_o} - (Z'+1)\, e^{-Z'} - Z_o\,(e^{-Z_o} - e^{-Z'}) + \frac{\Omega_o\, a^2}{\pi}\,(aZ'+1)\, e^{-aZ'} - \left(\frac{\Omega_o b}{2\pi}\right)^2 (bZ'+1)\, e^{-bZ'}\right] \quad , \tag{12}$$

where $a = 1 + 1/Z_1$ and $b = 1 + 2/Z_1$. Notice there are six parameters on which the flux depends: E_1, E', E_o, E_t, n, and M.

In the limit of a constant Ω $(=\Omega_o)$, E_1 goes to infinity, a and b go to 1, and equation (12) reduces to:

$$\text{Flux} = \frac{K}{2}\left[e^{-Z_o} - \cos^2\theta_o\, e^{-Z_o/\cos^2\theta_o}\right] \quad . \tag{13}$$

For limited but constant Ω, E' can be found analytically to be

$$E' = E_o/\cos^2\theta_o \qquad \text{and} \qquad \cos\theta_o = (1-\Omega_o/2\pi) \quad .$$

These last two equations were also used in reducing equation (12) to equation (13). Equation (13) can also be obtained by direct integration. For $\theta_o = 90°$, one obtains:

$$\text{Flux} = \frac{K}{2}\, e^{-Z_o} \quad . \tag{14}$$

Since the LIMS is geometrically limited in the acceptance cone, all comparisons using equation (12) will be made against equation (13).

From Figure 2, E_1 for H^+ and He^+ ions was estimated to be 17 and 6 eV, respectively. These two ions were used so that comparisons could be made with the spacecraft-mounted instrument. Two examples of fits to data will be shown later. For the moment, however, this report will concentrate on the instrumental effect on derived temperatures and densities.

In order to calculate the flux, it is clear from equation (12) that E' as a function of E_o must be known. Because of the form assumed for Ω, the equation for E' is a transcendental equation of the form:

$$\sqrt{E_o/E'} = 1-(\Omega_o/2\pi)\exp(E'/E_1) \quad . \tag{15}$$

The Z notation has been dropped in order to explicitly show the relationship between the energies.

This equation is solved graphically and a table of values of E' for the appropriate values of E_o and E_1 is generated. Figure 4 shows the graph used for H^+ (E_1 = 17 eV) to find the E', one for each E_o. A graph such as this would have to be generated for each mass; since, as noted earlier, E_1 varies with mass. Table 1 gives the values of E_o and E' used in the calculations that follow.

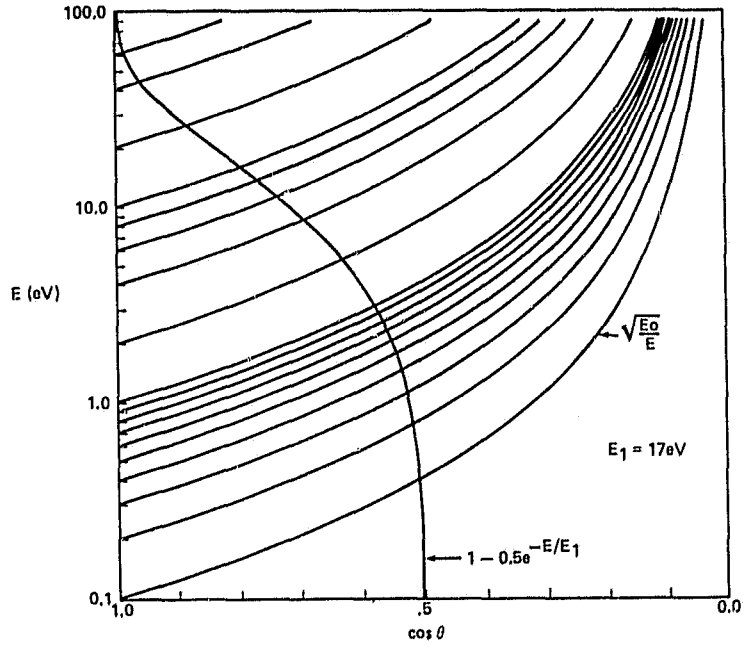

Figure 4. Graph of $\sqrt{E/E_o}$ and $1-(\Omega_o/2\pi)\exp(-E'/E_1)$ used to graphically find E'. For this set of curves E_1 = 17 eV.

A set of curves for several different thermal energies, E_t (=kT), was generated to see how the calculated flux varied as a result of the decrease in acceptance cone solid angle with energy (Instrumental Effect A). Figures 5 through 10 show the RPA curves, or plots of flux versus retarding potential, calculated for the LIMS using equation (12). Equation (13) was used to calculate a reference set of curves which are plotted in Figures 5 through 10 as dashed lines. The solid lines are the RPA curves determined with equation (12) and the data in Table 1. RPA curves are shown for H^+ (E_1 = 17 eV) in Figures 5 through 7, while Figures 8 through 10 show RPA curves for He^+ (E_1 = 6 eV). For each ion, three cases are presented:

$E_t << E1$

$E_t \approx E_1$

and

$E_t >> E_1$.

TABLE 1. VALUES OF E_o AND E' USED IN THE CALCULATIONS OF FLUX IN EQUATIONS (12) AND (13)

	H^+ (E_1 = 17 eV)	H_e^+ (E_1 = 6 eV)
E_o	E'	E'
0.0	0.00	0.00
0.2	0.74	0.36
0.4	1.40	0.66
0.6	1.99	1.16
0.8	2.50	1.59
1.0	2.95	1.98
2.0	5.01	2.30
4.0	8.35	3.73
6.0	11.00	6.00
8.0	13.60	8.00
10.0	16.00	9.81
20.0	26.00	11.60
40.0	44.00	20.80
60.0	62.00	

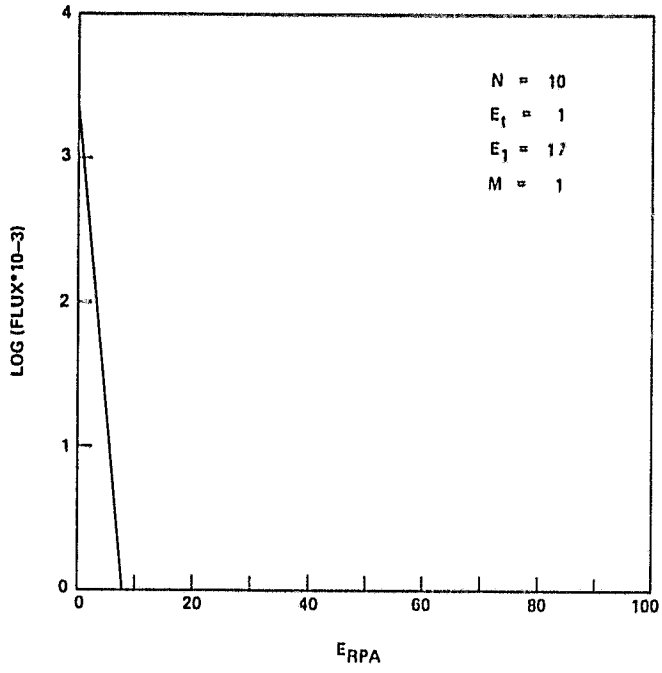

Figure 5. Plots of flux versus RPA for H^+ and E_t = 1 eV. The solid line is the flux calculated including Instrumental Effect A while the dashed line is the flux calculated with the reference equation.

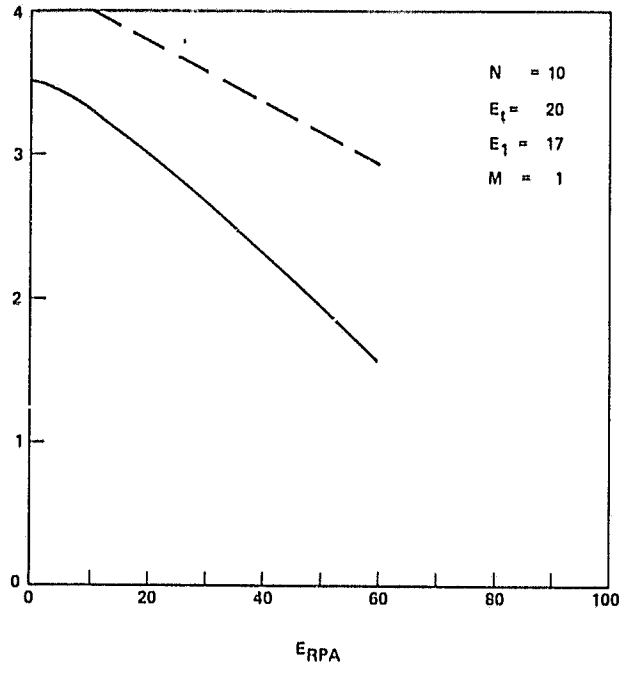

Figure 6. Plots of flux versus RPA for H^+ and E_t = 20 eV. The solid line is the flux calculated including Instrumental Effect A while the dashed line is the flux calculated with the reference equation.

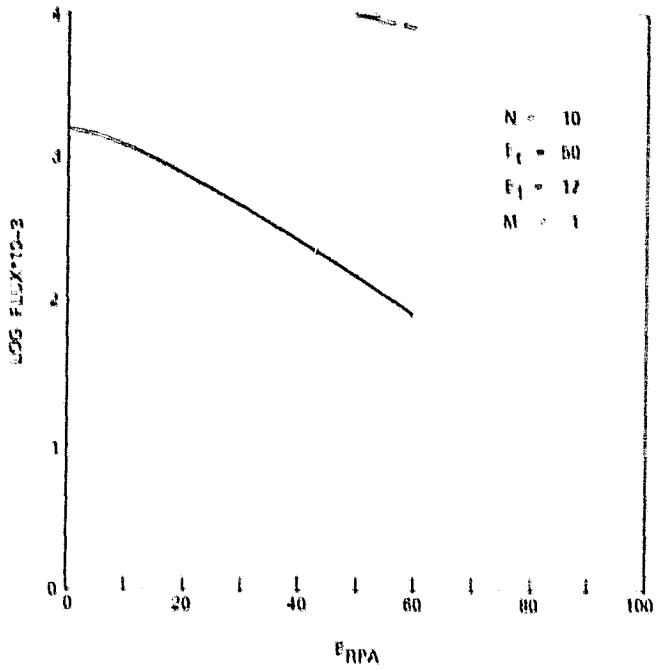

Figure 7. Plots of flux versus RPA for H^+ and E_t = 50 eV. The solid line is the flux calculated including Instrumental Effect A while the dashed line is the flux calculated with the reference equation.

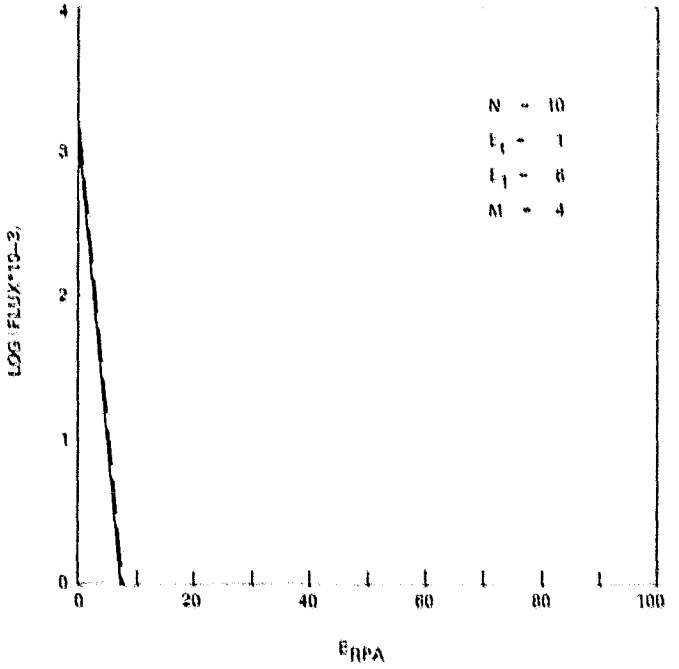

Figure 8. Plots of flux versus RPA for He^+ and E_t = 1 eV. The solid line is the flux calculated including Instrumental Effect A while the dashed line is the flux calculated with the reference equation.

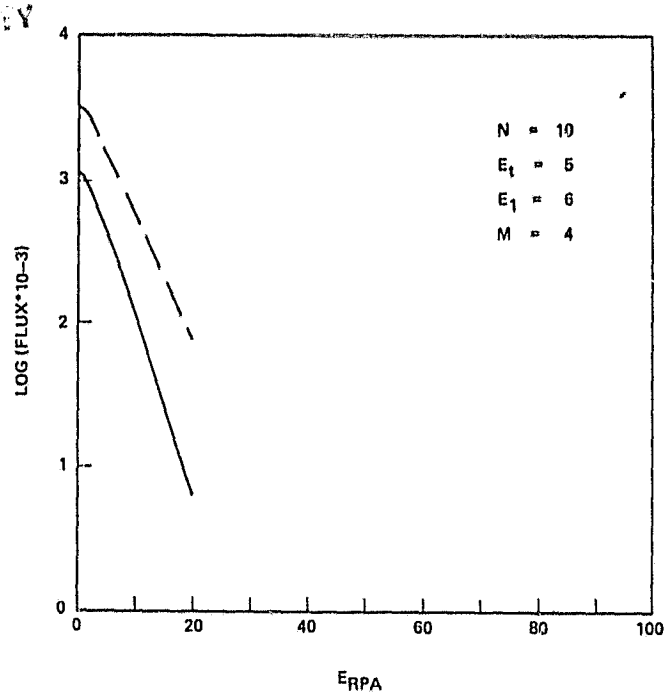

Figure 9. Plots of flux versus RPA for He^+ and E_t = 5 eV. The solid line is the flux calculated including Instrumental Effect A while the dashed line is the flux calculated with the reference equation.

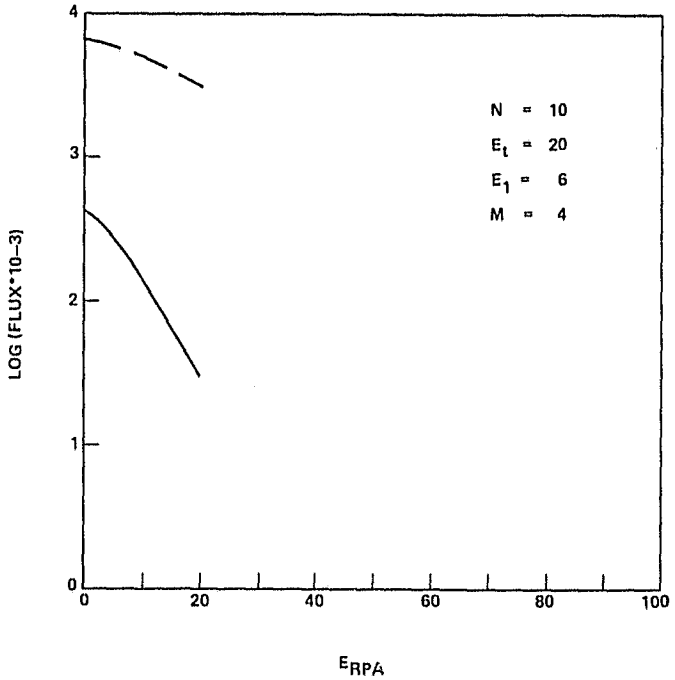

Figure 10. Plots of flux versus RPA for He^+ and E_t = 20 eV. The solid line is the flux calculated including Instrumental Effect A while the dashed line is the flux calculated with the reference equation.

Specifically, for H^+ (E_1 = 17 eV), E_t is set to 1, 20, and 50 eV in Figures 5, 6, and 7, respectively; while, for He^+ (E_1 = 6 eV), E_t is 1, 5, and 20 eV in Figures 8, 9, and 10, respectively.

One fact immediately clear from the figures is that once the thermal energy of the plasma is greater than E_1, the measured flux actually decreases with increasing thermal energy as a result of Instrumental Effect A. When the thermal energy is below E_1, the flux seen by the instrument does not increase as rapidly with E_t as does the flux affected only by a geometrically limited aperture. In fact, the flux increases relatively little in comparison to the reference. Also, the slope of the curve continuously changes with the retarding potential so that linear fits to the log of the flux are not appropriate and do not give valid results.

A grasp of the magnitude of the influence of Instrumental Effect A on flux measurements can be obtained by comparing the flux calculated with a constant acceptance solid angle with the flux calculated taking into account the decrease in solid angle with energy. Equation (13) gives the flux for constant acceptance cone solid angle, while equation (12) gives the flux for a decreasing solid angle. Consider the ratio R of equation (13) to equation (12). This ratio for zero RPA gives the full effect of the solid angle decrease on the flux. The ratio at zero RPA is:

$$R = (1 - \cos^2\theta_o)/(\Omega_o a^2/\pi - \Omega_o{}^2 b^2/4\pi^2) \quad . \tag{16}$$

For the LIMS $\theta_o = 60°$; therefore, $\Omega_o = \pi$, and equation (16) reduces to:

$$R = 0.75/(a^2 - b^2/4) \quad . \tag{17}$$

Table 2 gives the value of R for three ions for three values of E_t. For the higher mass ions at the higher temperatures the reduction in flux due to Instrumental Effect A is quite dramatic.

TABLE 2. RATIO OF FLUX AT ZERO RPA FOR NO EFFECT A TO FLUX AT ZERO RPA WITH EFFECT A

E_t (eV) \ Ion	H^+ E_1 = 17 eV	He^+ E_1 = 6 eV	O^+ E_1 = 4 eV
1	1.08	1.26	1.42
10	2.18	5.89	10.04
20	3.97	15.31	

INSTRUMENTAL EFFECT B

With the equation for the flux into the instrument [equation (12)], return to equation (4) and calculate the effects of a limited bandpass (Instrumental Effect B). From the form assumed for the bandpass, an obvious effect of the bandpass will be the reduction of the integral flux for the energies between E_L and infinity, where the flux would fall to 0 for $E_L = E_u$. Figure 11 shows the effect of bandpass widths of E_u = 8 and 6 eV on a Maxwellian plasma with E_t = 10 eV. The acceptance field-of-view is assumed to be hemispherical. If this effect were dominant, it too could affect the shape of the RPA curve as shown and therefore the derived temperatures and densities. Since RPA devices detect integral flux, then for a plasma which would be affected (depending on the thermal energy and the bandpass), the RPA curve would not start at as high a flux as expected and would fall off faster than expected if the bandpass upper energy limit were greater than the plasma thermal energy. The bandpass effect for the Maxwellian plasma is obvious in Figure 11. However, the effects on an RPA curve may be much more subtle in instruments for which other instrumental effects are working; e.g., Instrumental Effect A. It should be obvious that for plasmas with $E_t << E_u$, there would be no effect on the RPA curve. Such effects due to the band-pass limitation would only be seen for plasmas that would have portions of the flux versus RPA curve above $E_u (E_t \sim E_u)$ and in instruments for which $E_1 \geq E_u$.

On the LIMS instrument, the bandpass has little effect on the flux for He^+ and H^+ since $E_1 << E_u$ for both ions and the solid angle decrease is the dominant effect. It would be significant for O^+ for which $E_1 \sim 4$ eV and E_u = 6 eV. However, the

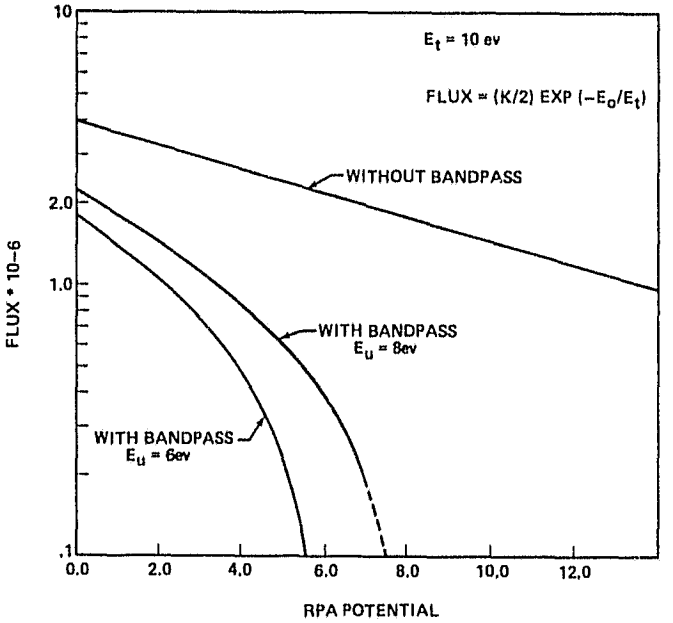

Figure 11. Comparison of the RPA curve with and without bandpass limits. Two RPA curves with bandpass limits of E_u = 8 and 6 eV are shown. A Maxwellian plasma with E_t = 10 eV was assumed. No other instrumental effects are included in these curves.

flux of O^+ into the instrument was never of such a magnitude that temperature or densities could be derived. Therefore, since that which follows is peculiar to the LIMS instrument, the bandpass effect will not be considered to be significant and is not included in the analysis.

EFFECT ON PARAMETERS DERIVED USING CURVE FIT ROUTINES

In a preliminary analysis of data from the LIMS, the function in equation (13) was used in a nonlinear least-squares fitting routine described by Bevington [2] to find the two parameters, temperature and density. To determine the error introduced by this procedure on the temperature and density derived, we used equation (13) to curve fit data calculated using equation (12). Such a procedure should show the effect of not including the decrease of the solid angle with energy (Instrumental Effect A) in the analysis. Figures 12 through 15 show the results of such fits as E_t is varied. In these figures, the points calculated with equation (12) and used as input data are shown as plus signs while the solid line is the curve calculated using equation (13) with the temperature and density to which the curve fit program converged in fitting the input data. In each figure, the input data is shown in the top line in the upper right-hand corner and the derived temperature and density in the bottom line. N is the input density, set to 10 in all the cases considered here, and M is the ion mass in amu's. A somewhat extensive set of curves is shown so that the behavior of the RPA curve with E_t can clearly be seen.

Both the thermal energy and density found with the curve fit routine rapidly diverge from the input values as the thermal energy increases. Figure 16 shows this result quite clearly. To generate this data, we used the derived temperature and density found as described earlier (Figs. 12 through 15). In the top panel of Figure 16, the derived temperature is plotted as a function of the real or input temperature. For an input temperature of about 12 eV, the derived temperature would be about 10 eV. The bottom panel of Figure 16 shows the ratio of the derived density to the input density as a function of input temperature. For example for an input temperature of about 10 eV, the derived density is about half the real density.

Good fits to the data can be obtained using equation (12) even with no correction for drift velocity or spacecraft charge. Figures 17 and 18 show such fits for two different plasmas encountered on SCATHA. The solid line in Figure 18 is the best fit curve; the data is represented by circles. One of the reasons for the difference between the best fit curve and the data at the higher energy is simply due to the choice for the lower cutoff in counts. We have chosen it very near the noise limit and in fact are probably in the noise for counts less than about 10. Because of the effect on temperature and density shown in Figure 16, temperature and densities for the LIMS data are now derived by curve fitting equation (12) to the data. One must be cautious, however, in quoting temperatures and densities when the derived temperature of the plasma is larger than E_1. When this condition is met, equation (12) becomes somewhat insensitive to temperature because now the solid angle decrease has an increasing effect compared to the RPA curve (compare the bottom two panels in Figure 15).

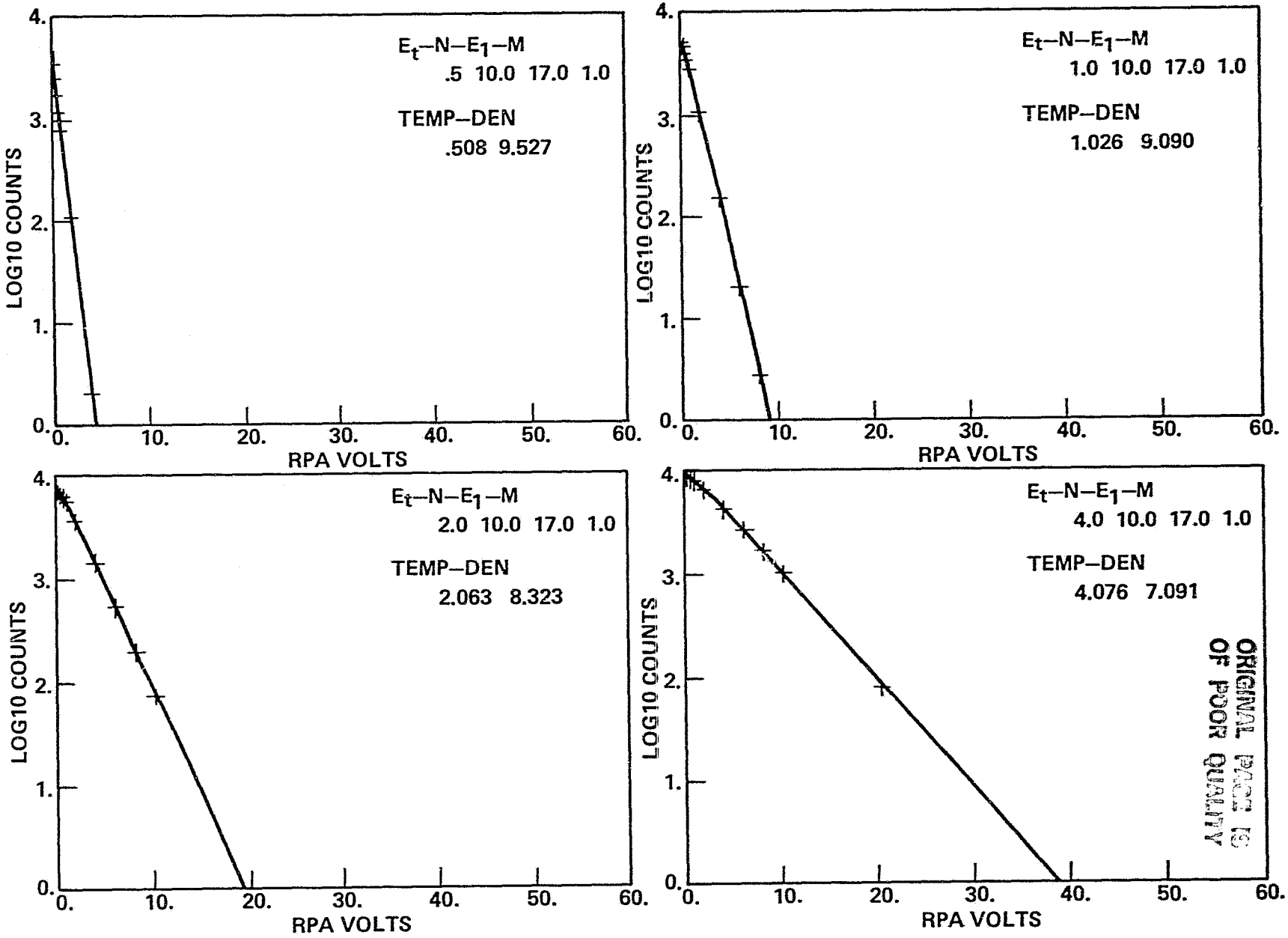

Figure 12. Plots of flux versus RPA potential for data calculated from equation (12) and fit with equation (13). The solid line is the best fit curve. The input and output parameters are shown in the upper right-hand corner of each panel. Here E_t(input) = 0.5, 1, 2, and 4 eV.

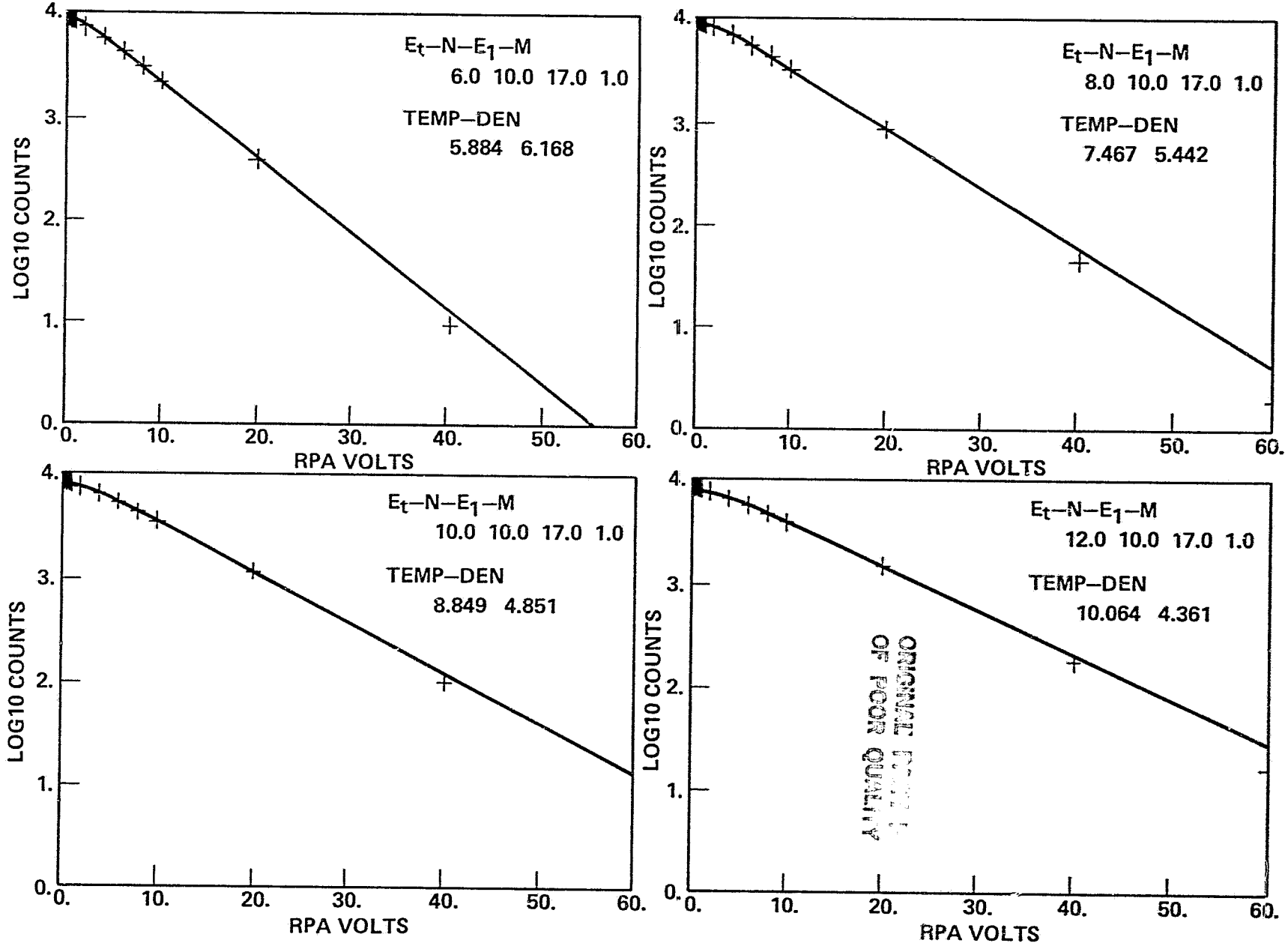

Figure 13. Plots of flux versus RPA potential for data calculated from equation (12) and fit with equation (13). The solid line is the best fit curve. The input and output parameters are shown in the upper right-hand corner of each panel. Here E_t(input) = 6, 8, 10, and 12 eV.

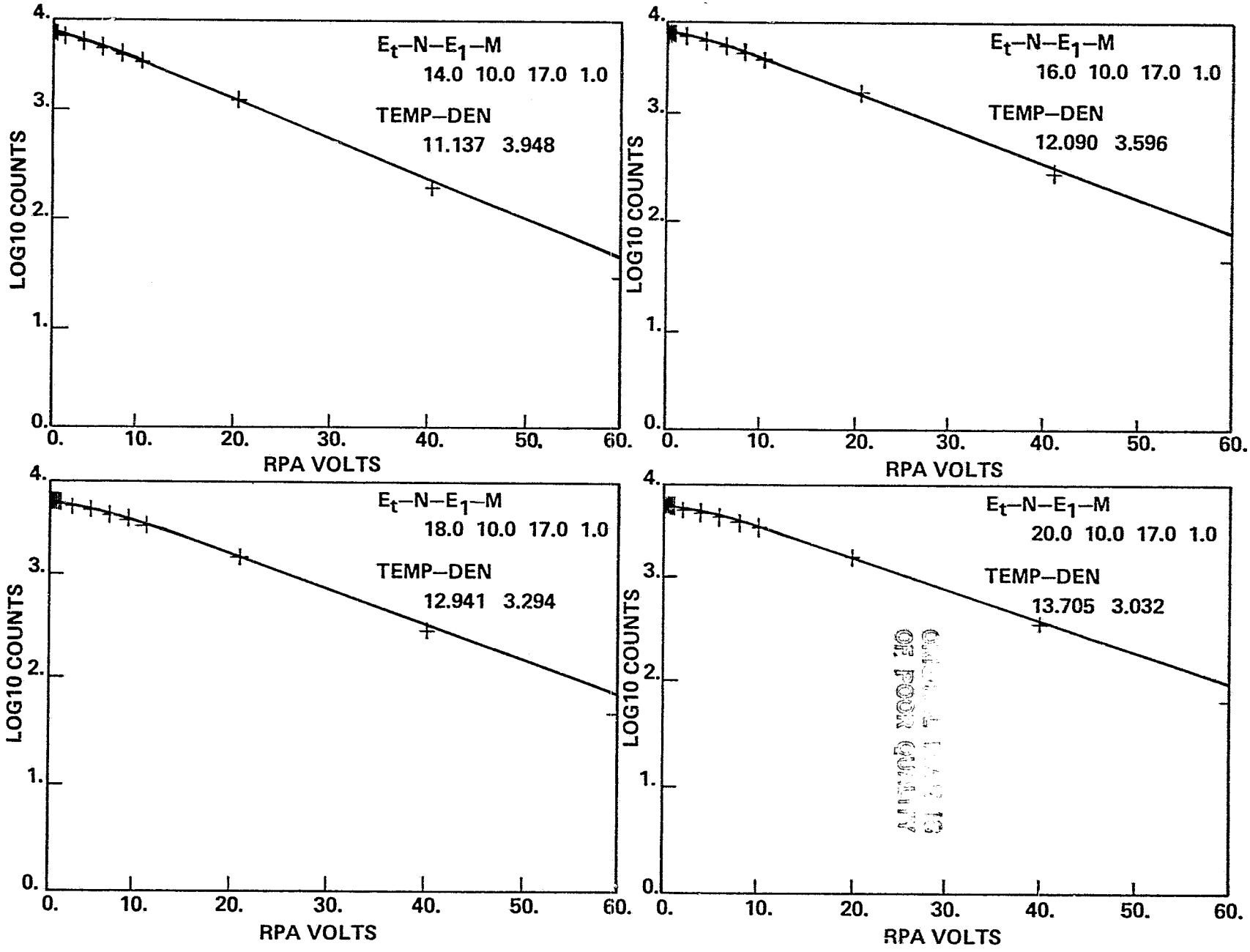

Figure 14. Plots of flux versus RPA potential for data calculated from equation (12) and fit with equation (13). The solid line is the best fit curve. The input and output parameters are shown in the upper right-hand corner of each panel. Here E_t(input) = 14, 16, 18, and 2ᴜ eV.

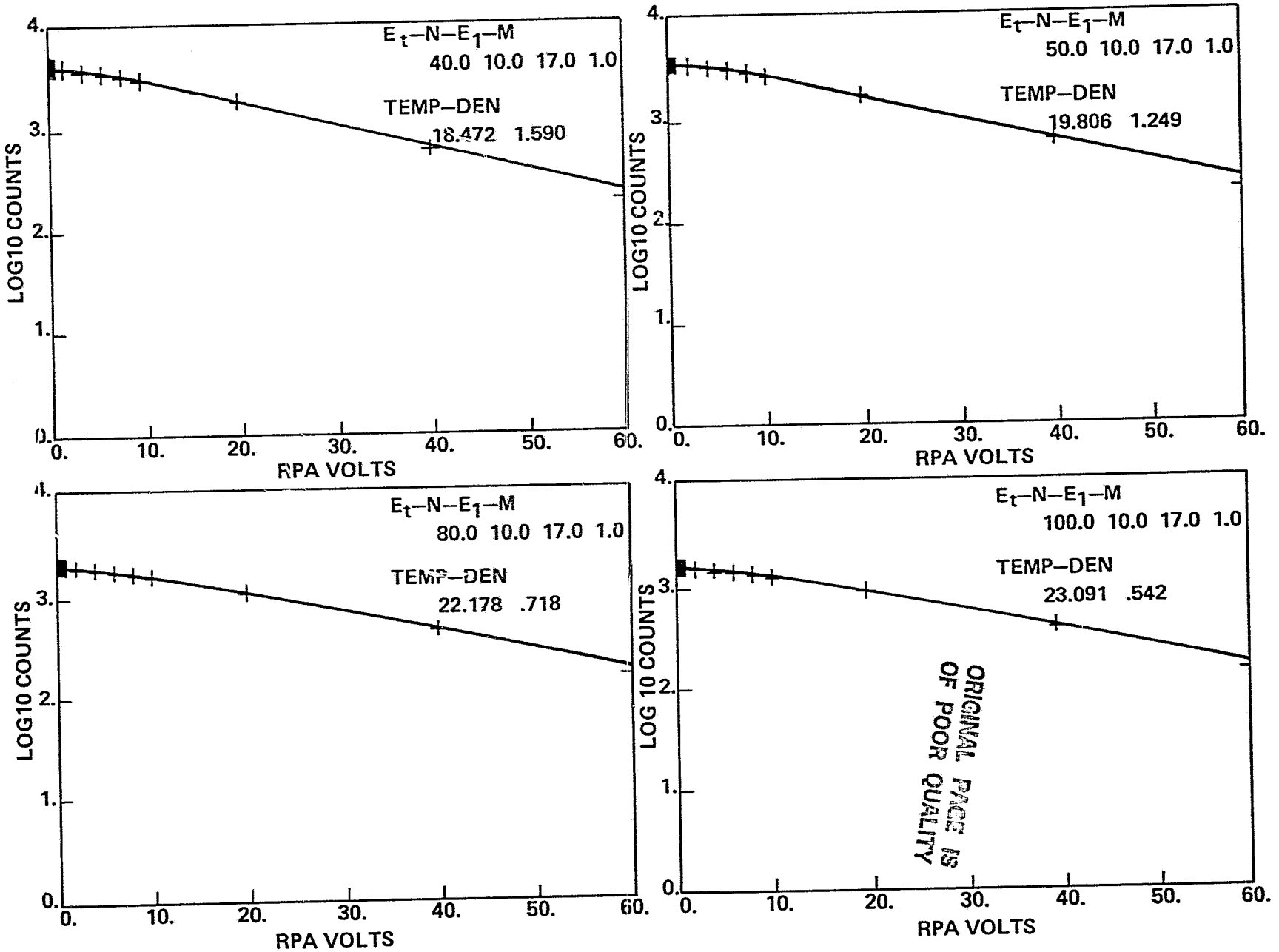

Figure 15. Plots of flux versus RPA potential for data calculated from equation (12) and fit with equation (13). The solid line is the best fit curve. The input and output parameters are shown in the upper right-hand corner of each panel. Here E_t(input) = 40, 50, 80, and 100 eV.

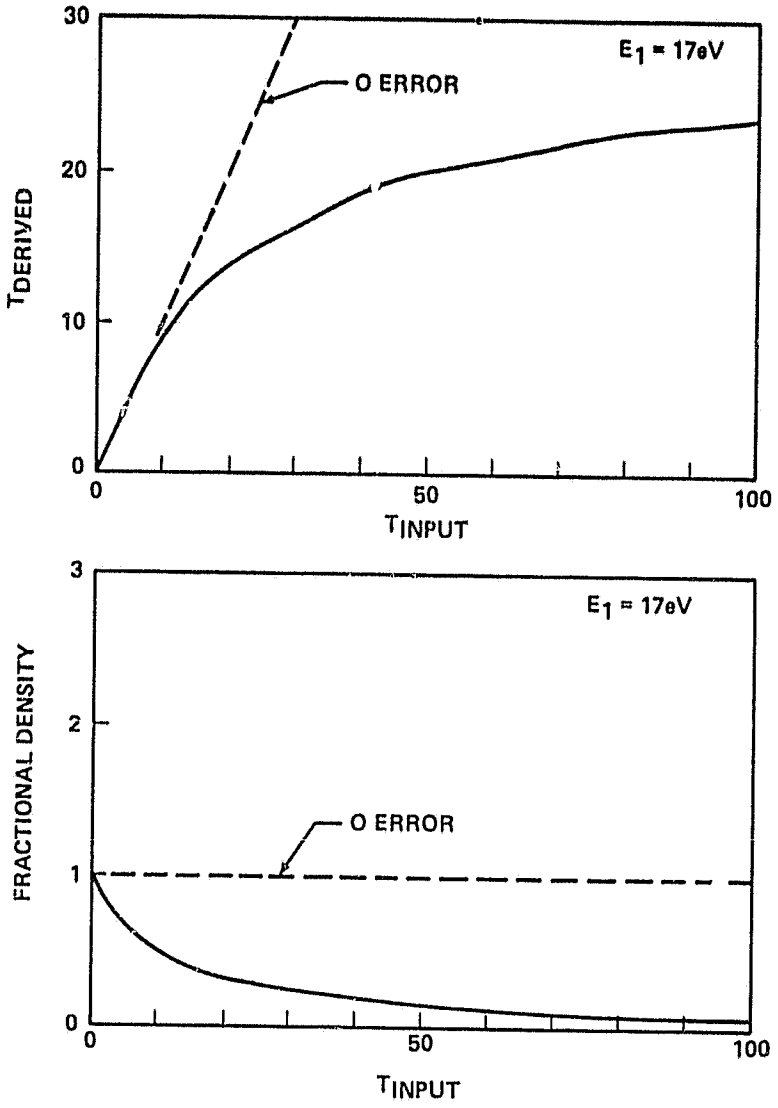

Figure 16. Summary of the derived temperatures and densities versus E_t. The top panel shows the derived temperature versus the input temperature. In the bottom panel is shown the fraction of the derived density to input density versus input temperature.

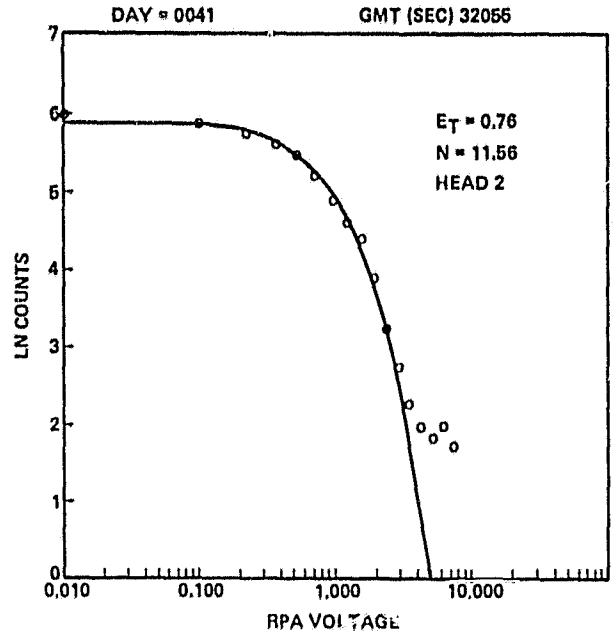

Figure 17. Example using equation (12) of a fit to data from the spacecraft instrument. This is an example of a cool plasma with $E_t = 0.76$. The solid line is the best fit curve represented by $E_t = 0.76$ and $N = 11.56$. The actual data is represented by the circles.

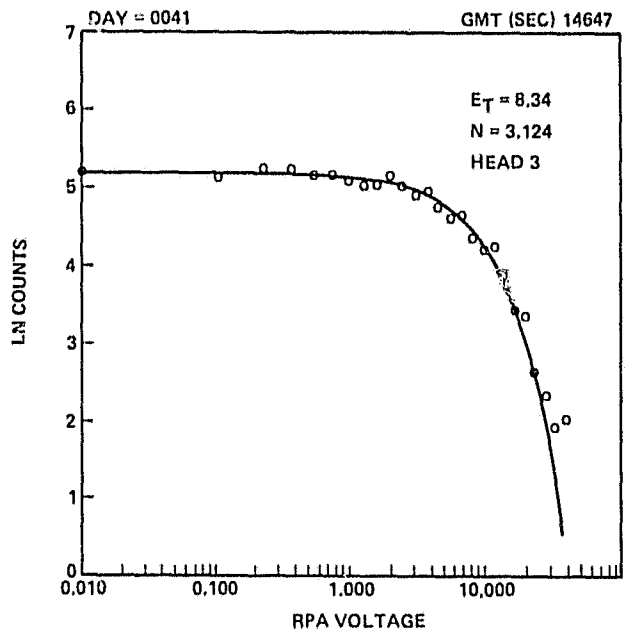

Figure 18. Example using equation (12) of a fit to data from the spacecraft instrument. This is an example of a warm plasma with $E_t = 8.34$. The solid line is the best fit curve represented by $E_t = 8.34$ and $N = 3.124$. The actual data is represented by the circles.

SUMMARY

An expression for the flux into a RPA is derived which takes into account the instrumental effect of a dependence on energy of the solid angle of the acceptance cone. A second instrumental effect of a limited bandpass is briefly discussed. It is shown that temperatures and densities derived without considering the effect of the solid angle dependence on energy will be too low, dramatically so for $E_t > E_1$, the e folding distance of the solid angle dependence. For $E_t << E_1$, there is effectively no impact on the derived temperatures and densities if the solid angle effect is ignored.

Bandpass limits can alter the RPA curves further if both E_t and E_1 are greater than the upper bandpass limit, E_u. Thus, when either E_1 or E_t approach E_u, one must check to determine the effect of the bandpass limits. On LIMS, the bandpass would affect only the RPA curves for O^+, since for O^+ $E_1 = 4$ eV and $E_u = 6$ eV.

REFERENCES

1. Reasoner, D. L., Chappell, C. R., Fields, S. A., Lewter, W. J.: Light Ion Mass Spectrometer for Space Plasma Investigations. Review of Scientific Instruments, Vol. 53, 1982, p. 441.

2. Bevington, Philip R.: Data Reduction and Error Analysis for the Physical Sciences. McGraw Hill Book Company, New York, New York, Chapter 11, 1969.

APPROVAL

INSTRUMENTAL EFFECTS ON THE TEMPERATURE AND DENSITY DERIVED FROM THE LIGHT ION MASS SPECTROMETER

By Paul D. Craven and David L. Reasoner

The information in this report has been reviewed for technical content. Review of any information concerning Department of Defense or nuclear energy activities or programs has been made by the MSFC Security Classification Officer. This report, in its entirety, has been determined to be unclassified.

A. J. DESSLER
Director, Space Science Laboratory

☆ U.S. GOVERNMENT PRINTING OFFICE: 1983—646-058/10